MIT Libraries | DSpace@MIT

MIT Open Access Articles

An Interhemispheric Four-Box Model of the Meridional Overturning Circulation

The MIT Faculty has made this article openly available. ***Please share*** how this access benefits you. Your story matters.

Citation: Stone, Peter H., and Yuriy P. Krasovskiy. "An Interhemispheric Four-Box Model of the Meridional Overturning Circulation." Journal of Physical Oceanography 41 (2011): 516-530. Web. 19 Oct. 2011. © 2011 American Meteorological Society

As Published: http://dx.doi.org/10.1175/2009jpo4123.1

Publisher: American Meteorological Society

Persistent URL: http://hdl.handle.net/1721.1/66498

Version: Final published version: final published article, as it appeared in a journal, conference proceedings, or other formally published context

Terms of Use: Article is made available in accordance with the publisher's policy and may be subject to US copyright law. Please refer to the publisher's site for terms of use.

Massachusetts Institute of Technology

An Interhemispheric Four-Box Model of the Meridional Overturning Circulation

PETER H. STONE AND YURIY P. KRASOVSKIY

Center for Global Change Science, Massachusetts Institute of Technology, Cambridge, Massachusetts

(Manuscript received 15 August 2008, in final form 15 April 2009)

ABSTRACT

The authors introduce a four-box interhemispheric model of the meridional overturning circulation. A single box represents high latitudes in each hemisphere, and in contrast to earlier interhemispheric box models, low latitudes are represented by two boxes—a surface box and a deep box—separated by a thermocline in which a balance is assumed between vertical advection and vertical diffusion. The behavior of the system is analyzed with two different closure assumptions for how the low-latitude upwelling depends on the density contrast between the surface and deep low-latitude boxes. The first is based on the conventional assumption that the diffusivity is a constant, and the second on the assumption that the energy input to the mixing is constant.

There are three different stable equilibrium states that are closely analogous to the three found by Bryan in a single-basin interhemispheric ocean general circulation model. One is quasi-symmetric with downwelling in high latitudes of both hemispheres, and two are asymmetric solutions, with downwelling confined to high latitudes in one or the other of the two hemispheres. The quasi-symmetric solution becomes linearly unstable for strong global hydrological forcing, while the two asymmetric solutions do not.

The qualitative nature of the solutions is generally similar for both the closure assumptions, in contrast to the solutions in hemispheric models. In particular, all the stable states can be destabilized by finite amplitude perturbations in the salinity or the hydrological forcing, and transitions are possible between any two states. For example, if the system is in an asymmetric state, and the moisture flux into the high-latitude region of downwelling is slowly increased, for both closure assumptions the high-latitude downwelling decreases until a critical forcing is reached where the system switches to the asymmetric state with downwelling in the opposite hemisphere. By contrast, in hemispheric models with the energy constraint, the downwelling increases and there is no loss of stability.

1. Introduction

The ocean circulation transports about 2 PW of heat poleward in the Northern Hemisphere (Ganachaud and Wunsch 2003) and thereby has a major effect on global and regional climate (Seager et al. 2002). The largest part of this heat transport is associated with the meridional overturning circulation (MOC) in the North Atlantic Ocean. There is considerable evidence that this circulation has undergone major changes in past climates (e.g., Broecker 2003, and references therein) and studies with a large variety of ocean models have shown that this circulation can have multiple equilibria and may be sensitive to the forcing by surface fluxes of heat and moisture (e.g., Bryan 1986; Marotzke and Willebrand 1991; Rahmstorf 1995). However, there is very little quantitative agreement between models about how sensitive this circulation is to changes in these surface fluxes (Rahmstorf et al. 2005; Stouffer et al. 2006).

The great majority of the studies that have investigated the sensitivity of the MOC has implicitly or explicitly represented turbulent vertical mixing by a fixed diffusivity. This mixing is responsible for injecting heat from the surface into the deep oceans in low latitudes, thereby creating the deep meridional density gradients that drive the MOC. The MOC is particularly sensitive to the diffusivity in the thermocline (Scott and Marotzke 2002; Bugnion et al. 2006), where it is believed to have as its primary source surface winds (Munk and Wunsch 1998). Since surface winds are likely to change when climate changes, investigations of the sensitivity of the MOC that fix the diffusivity may not be realistic.

Corresponding author address: Dr. Peter H. Stone, Massachusetts Institute of Technology, Room 54-1718, Cambridge, MA 02142.
E-mail: phstone@mit.edu

DOI: 10.1175/2009JPO4123.1

© 2011 American Meteorological Society

An alternate approach has been suggested by Huang (1999) and Nilsson and Walin (2001), namely, that one could assume that the energy input to the mixing is constant, rather than the diffusivity. One would expect that this energy input, like the diffusivity, is susceptible to climate change, so there is no a priori reason why either assumption should be more realistic. This uncertainty is potentially important because the two different approaches lead to strikingly different sensitivities in hemispheric models. In both cases the MOC exhibits two different stable equilibria—a thermally dominated state corresponding to the current climate and a salinity-dominated state. In the case of constant diffusivity when the moisture flux into high latitudes increases, the strength of the thermally dominated state decreases, and for sufficiently strong forcing it collapses to the salinity-dominated state. In contrast, when one assumes constant energy input the MOC increases in strength when the moisture flux into high latitudes increases and there is no collapse (Huang 1999; Nilsson and Walin 2001; Nilsson et al. 2003; Mohammad and Nilsson 2004).

However, the circulation and transports in the Atlantic are interhemispheric (e.g., Ganachaud and Wunsch 2003), and thus a realistic comparison of the two constraints requires an interhemispheric model. Two studies have addressed this issue in part, namely those of Nilsson et al. (2004) and Marzeion et al. (2007). The former used both an ocean general circulation model (OGCM) with a single interhemispheric basin and an analogous box model in their analyses, but their results were limited by the fact that they examined only solutions that were symmetric about the equator. They found the same contrast in the responses of the MOC to increases in the high-latitude moisture fluxes as in the hemispheric models. They also found that the symmetric solutions were unstable when the salinity contrasts exceed a critical value, and that asymmetric perturbations dominated the instability. However, they did not examine what kind of asymmetric solutions might exist, and what their stability properties might be. We know that stable asymmetric solutions do exist in models of a single interhemispheric basin with the diffusivity constraint. They exist both in box models (Rooth 1982; Scott et al. 1999) and in OGCMs (Bryan 1986). These solutions are clearly more realistic than those considered by Nilsson et al. (2004). We also note that both Bryan (1986) and Marotzke and Klinger (2000) found a stable symmetric solution in their single-basin interhemispheric OGCMs.

In the second study, Marzeion et al. (2007) used a global OGCM with a stratification-dependent diapycnal diffusivity to examine how the Atlantic MOC responds to an anomalous flux of freshwater into the North Atlantic.

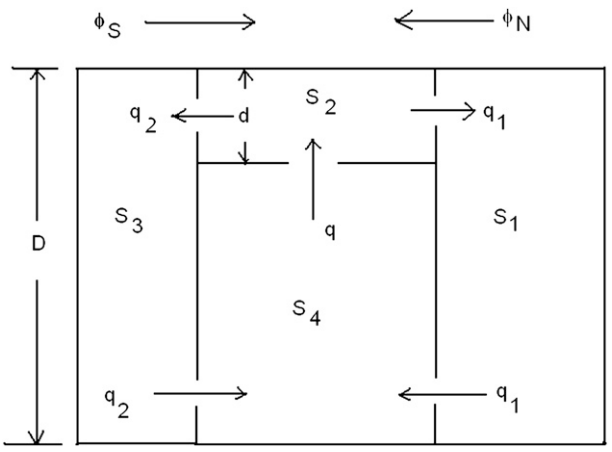

FIG. 1. Schematic of the four-box model.

They found that the response in the case corresponding to a constant energy input was a decrease in the Atlantic MOC, in contrast to the Nilsson et al. (2004) result. They did not identify the cause of this difference, but one obvious possible cause was that Marzeion et al.'s MOC was asymmetric.

Thus to understand better what kind of states can exist in an interhemispheric basin and how their behavior depends on the representation of the diffusivity, we introduce a new and more general interhemispheric box model. The model has four boxes: two separate high-latitude boxes (one in each hemisphere) and two low-latitude boxes (one representing near-surface conditions and the other the deep ocean). This makes it possible to include an explicit representation of the low-latitude upwelling, which has been omitted in many classic box models (e.g., Stommel 1961; Rooth 1982). It also allows an explicit representation of the balance between vertical advection and vertical diffusion in the thermocline. Finally, another feature that distinguishes our analysis from that of Nilsson et al. (2004) is that they assumed that the depth of the low-latitude surface layer is small compared to the ocean depth, whereas we do not.

The paper is organized as follows: the model is described in section 2; its equilibrium solutions are derived and described in section 3; the stability properties of the solutions are described in section 4; hysteresis loops describing the model's response to ''hosing'' experiments are derived in section 5; and the results are summarized and discussed in section 6.

2. Model description

We consider a two-hemisphere ocean box model. The geometry of the model is shown in Fig. 1. Boxes 1 and 3 are northern and southern high latitudes with equal

volumes. Boxes 2 and 4 are the tropical boxes. The ratio of the sum of the two equatorial boxes' volumes to the high-latitude box volume is defined as V. Box 2 represents an upper thermocline layer with depth d overlying an abyssal layer represented by box 4. The total depth of boxes 1 and 3 is D. The boxes are well mixed. Temperature, salinity, and density of box i are T_i, S_i, and ρ_i, respectively. The fractional volume flux from box 4 to box 2 is q, and the fractional volume fluxes between the high- and low-latitude boxes are denoted by q_1 and q_2, with positive values corresponding to sinking in high latitudes. Finally, ϕ_N and ϕ_S represent virtual salinity fluxes from high to low latitudes, equivalent to moisture fluxes from low to high latitudes.

To a first approximation, the effect of the thermohaline circulation on the temperature of boxes 1, 2, and 3 is weak compared to the effect of surface heat fluxes (Krasovskiy and Stone 1998) and we therefore fix T_1, T_2, and T_3. Furthermore we will assume that the thermal forcing is symmetric (i.e., $T_1 = T_3$). Thus, ultimately the deep low-latitude box must assume the same temperature as the high-latitude boxes and we need only distinguish the two temperatures T_2 and T_4.

We parameterize the volume fluxes from classical thermocline scaling, as derived by Nilsson and Walin (2001). This assumes a balance in the thermocline between vertical advection by upwelling and downward vertical diffusion. The two cases of constant diffusivity and constant flux of energy across the interface between boxes 2 and 4 can be represented simultaneously:

$$q = 2k\left(\frac{\rho_{42}}{\rho_{420}}\right)^{-n}\left(\frac{h}{h_0}\right)^{-1}, \tag{1}$$

$$q_1 = k\left(\frac{\rho_{12}}{\rho_{120}}\right)\left(\frac{h}{h_0}\right)^{2}, \tag{2}$$

$$q_2 = k\left(\frac{\rho_{32}}{\rho_{320}}\right)\left(\frac{h}{h_0}\right)^{2}, \tag{3}$$

where

$$\rho_{ij} = \rho_i - \rho_j, \quad i, j = 1, \ldots, 4, \tag{4}$$

$$h = \frac{d}{D}. \tag{5}$$

The subscript "0" refers to reference values, which we will base on an equilibrium state, to be specified later, and k is an empirical coefficient that we will use to tune the model appropriately for this reference state.

Note that we have assumed that boxes 1 and 3 are geometrically identical, so that the same coefficient, k, is used in both hemispheres; and we have made use of the fact that in equilibrium $q = q_1 + q_2$. For a constant diffusivity $n = 0$, while for a constant energy flux $n = 1$ (Nilsson and Walin 2001). Assuming a linear equation of state, we can rewrite Eq. (4) as

$$\rho_{ij} = \alpha(T_j - T_i) + \beta(S_i - S_j), \tag{6}$$

where α and β are, respectively, constant thermal and haline expansion coefficients. We also define temperature and salinity contrasts characterizing low latitudes:

$$\Delta T = T_2 - T_4, \quad \Delta S = S_{20} - S_{40}, \quad r = \frac{\beta \Delta S}{\alpha \Delta T}. \tag{7}$$

The salt conservation equations for the model and the equation for the depth of the thermocline now assume the form

$$\frac{dS_1}{dt} = Q_1 - \phi_N; \tag{8}$$

$$\frac{dS_2}{dt} = \frac{1}{hV}Q_2 + \frac{\phi_N + \phi_S}{hV}; \tag{9}$$

$$\frac{dS_3}{dt} = Q_3 - \phi_S; \tag{10}$$

$$\frac{dS_4}{dt} = \frac{1}{(1-h)V}Q_4; \tag{11}$$

$$\frac{dh}{dt} = \frac{1}{V}(q - q_1 - q_2); \tag{12}$$

where

$$Q_1 = \begin{cases} q_1(S_2 - S_1), & \text{if} \quad q_1 > 0; \\ -q_1(S_4 - S_1), & \text{if} \quad q_1 < 0; \end{cases} \tag{13}$$

$$Q_2 = \begin{cases} q(S_4 - S_2), & \text{if} \quad q_1 > 0, q_2 > 0; \\ q(S_4 - S_2) - q_2(S_3 - S_2), & \text{if} \quad q_1 > 0, q_2 < 0; \\ q(S_4 - S_2) - q_1(S_1 - S_2), & \text{if} \quad q_1 < 0, q_2 > 0; \\ q(S_4 - S_2) - q_1(S_1 - S_2) - q_2(S_3 - S_2), & \text{if} \quad q_1 < 0, q_2 < 0; \end{cases} \tag{14}$$

$$Q_3 = \begin{cases} q_2(S_2 - S_3), & \text{if} \quad q_2 > 0; \\ -q_2(S_4 - S_3), & \text{if} \quad q_2 < 0; \end{cases} \tag{15}$$

$$Q_4 = \begin{cases} q_1(S_1 - S_4) + q_2(S_3 - S_4), & \text{if} \quad q_1, q_2 > 0; \\ q_1(S_1 - S_4), & \text{if} \quad q_1 > 0, q_2 < 0; \\ q_2(S_3 - S_4), & \text{if} \quad q_1 < 0, q_2 > 0; \\ 0, & \text{if} \quad q_1 < 0, q_2 < 0. \end{cases} \tag{16}$$

Next we put the equations into nondimensional form. We define nondimensional variables:

$$t^* = 2kt, \quad S_i^* = \frac{S_i}{\Delta S}, \tag{17}$$

$$\phi_{N,S}^* = \frac{\phi_{N,S}}{2k\Delta S}; \quad q^*, q_1^*, q_2^* = \frac{1}{2k}(q, q_1, q_2), \tag{18}$$

and

$$Q_n^* = \frac{Q_n}{2k\Delta S}, \quad n = 1, 2, 3, 4. \tag{19}$$

Substituting these into Eqs. (8)–(12), and now dropping the asterisks, we find the following nondimensional equations:

$$\frac{dS_1}{dt} = Q_1 - \phi_N, \tag{20}$$

$$\frac{dS_2}{dt} = \frac{1}{hV}[Q_2 + \phi_N + \phi_S], \tag{21}$$

$$\frac{dS_3}{dt} = Q_3 - \phi_S, \tag{22}$$

$$\frac{dS_4}{dt} = \frac{1}{(1-h)V} Q_4, \tag{23}$$

$$\frac{dh}{dt} = \frac{1}{V}(q - q_1 - q_2). \tag{24}$$

We note that the relations between the Q_is, the qs, and the S_is in nondimensional form are identical to the dimensional forms given in Eqs. (13)–(16). Also, Eqs. (1)–(3) can be rewritten in nondimensional form, using the notation $S_{ij} = S_i - S_j$, as follows:

$$q = \left(\frac{1 - rS_{24}}{1 - r}\right)^{-n} \left(\frac{h}{h_0}\right)^{-1}, \tag{25}$$

$$q_1 = \frac{1}{2}\left(\frac{1 - rS_{21}}{1 - rS_{210}}\right)\left(\frac{h}{h_0}\right)^2, \tag{26}$$

$$q_2 = \frac{1}{2}\left(\frac{1 - rS_{23}}{1 - rS_{230}}\right)\left(\frac{h}{h_0}\right)^2, \tag{27}$$

where

$$S_{ij} = S_i - S_j, \quad S_{ij0} = S_{i0} - S_{j0}. \tag{28}$$

Note that, because of Eq. (7),

$$S_{240} = 1. \tag{29}$$

3. Equilibrium solutions

The external forcing for the system is given by the temperatures of the boxes, T_i, and by the virtual salinity fluxes, ϕ_N and ϕ_S. Because of our assumed symmetry for the thermal forcing, the effect of the temperatures can be characterized by ΔT, or in nondimensional form, by r [Eq. (7)]. If we make choices for ΔT and ΔS based on observations of the Atlantic, for example, $\Delta T \simeq 15$ K, $\Delta S \simeq 0.5$ psu, $\alpha = 1.5 \times 10^{-4}$ K^{-1}, $\beta = 8 \times 10^{-4}$ (psu)$^{-1}$, then $r \simeq 0.2$. Thus we shall use $r = 0.2$ for our numerical calculations. We note that Nilsson et al. (2004) found that symmetric solutions were stable only if $r < 0.5$. Also we will take $V = 2$ in all our calculations.

Since the important difference between the diffusivity and energy constraints is the behavior of the solutions when the global moisture fluxes into high latitudes increase, we will derive the solutions for arbitrary values of the total moisture flux. However, in order to limit the complexity of the analysis, we will only illustrate equilibrium solutions for two choices for the ratio of the moisture fluxes in the two hemispheres. One will be $\phi_n = \phi_S$, in which case all the forcing is symmetric about the equator, and we anticipate that symmetric solutions will exist. The second choice will be $\phi_N = 1.5\phi_S$, in which case we do not expect to find purely symmetric solutions. This second choice is motivated by the observed asymmetry in the moisture fluxes into the North and South Atlantic (Broecker et al. 1990).

To obtain steady-state solutions $\overline{S}_i$, $\overline{h}$, we can write Eqs. (8)–(12) in the form

$$Q_1(\overline{S}_i) = \phi_N, \tag{30}$$

$$Q_2(\overline{S}_i) = -(\phi_n + \phi_S), \tag{31}$$

$$Q_3(\overline{S}_i) = \phi_S, \tag{32}$$

$$Q_4(\overline{S}_i) = 0, \tag{33}$$

$$\overline{q} = \overline{q}_1 + \overline{q}_2, \tag{34}$$

where $\overline{q}$, $\overline{q}_1$, $\overline{q}_2$, $\overline{S}_i$ are steady-state values of q, q_1, q_2, S_i, respectively. From Eqs. (30) and (32) we obtain

$$\frac{Q_1(\overline{S})}{Q_3(\overline{S})} = \kappa, \tag{35}$$

where

$$\kappa \equiv \frac{\phi_N}{\phi_S}. \tag{36}$$

We express the depth of the upper layer in terms of salinity differences using Eqs. (25)–(27) and (34):

$$\frac{\overline{h}}{h_0} = \left\{\left(\frac{1-r\overline{S}_{24}}{1-r}\right)^n \left[\frac{1}{2}\left(\frac{1-r\overline{S}_{21}}{1-rS_{210}}\right) + \frac{1}{2}\left(\frac{1-r\overline{S}_{23}}{1-rS_{230}}\right)\right]\right\}^{-1/3}. \tag{37}$$

We introduce a new variable z:

$$z = \frac{\overline{S}_{23}}{\overline{S}_{21}}. \tag{38}$$

We can reduce the system of Eqs. (30)–(34) to two simultaneous equations for z and $\overline{S}_{24}$. To do this we consider the following three cases separately:

$$\begin{aligned} &\text{Case 1: } \overline{q}_1 > 0, \quad \overline{q}_2 > 0;\\ &\text{Case 2: } \overline{q}_1 > 0, \quad \overline{q}_2 < 0;\\ &\text{Case 3: } \overline{q}_1 < 0, \quad \overline{q}_2 > 0. \end{aligned}$$

There are no equilibrium solutions if $q_1 < 0$, $q_2 < 0$.

a. Case 1

From Eqs. (13) to (15), (30) to (32), (34), (35), and (38), we can find $\overline{S}_{21}$ and $\overline{S}_{23}$ in the forms

$$\overline{S}_{23} = \overline{S}_{24}\frac{\kappa z + 1}{\kappa + 1}, \tag{39}$$

$$\overline{S}_{21} = \overline{S}_{24}\frac{\kappa z + 1}{(\kappa + 1)z}. \tag{40}$$

To express $\overline{S}_{24}$ in terms of z, write the ratio $\overline{q}_1/\overline{q}_2$ using Eqs. (26) and (27). We obtain

$$\frac{\overline{q}_1}{\overline{q}_2} = l\frac{1-r\overline{S}_{21}}{1-r\overline{S}_{23}}, \tag{41}$$

where

$$l = \frac{1-rS_{230}}{1-rS_{210}}. \tag{42}$$

Note from Eqs. (13), (15), and (38) that we can write Eq. (35) in the form

$$\frac{\overline{q}_1}{\overline{q}_2} = \kappa z. \tag{43}$$

Equating the right-hand sides of Eqs. (41) and (43), and substituting for $\overline{S}_{21}$ and $\overline{S}_{23}$ from Eqs. (39) and (40), we obtain

$$\overline{S}_{24} = \frac{(\kappa z - l)(\kappa + 1)z}{(\kappa z^2 - l)(\kappa z + 1)r}. \tag{44}$$

We derive the second equation for $\overline{S}_{24}$ and z as follows: rewrite Eq. (31) in the form

$$\overline{q}\overline{S}_{24} = \phi_N + \phi_S, \tag{45}$$

substitute Eq. (37) for $\overline{h}$ into Eq. (25), and substitute the resulting equation for $\overline{q}$ into Eq. (45). We obtain

$$\begin{aligned} \overline{S}_{24} = (\phi_N + \phi_S)&\left(\frac{1-r\overline{S}_{24}}{1-r}\right)^{2n/3}\\ &\times\left\{\frac{1}{2}\left[\frac{(\kappa+1)z - r\overline{S}_{24}(\kappa z+1)}{(\kappa+1)z(1-rS_{210})}\right]\right.\\ &\left.+\frac{1}{2}\left[\frac{\kappa+1-r\overline{S}_{24}(\kappa z+1)}{(\kappa+1)(1-rS_{230})}\right]\right\}^{-1/3}. \end{aligned} \tag{46}$$

Equations (44) and (46) can be solved simultaneously for $\overline{S}_{24}$ and z. Equations (39) and (40) then give us $\overline{S}_{21}$ and $\overline{S}_{23}$, Eq. (37) gives us $\overline{h}$, and Eqs. (25)–(27) give us $\overline{q}$, $\overline{q}_1$, and $\overline{q}_2$. Note that h must satisfy

$$0 < h < 1. \tag{47}$$

For convenience, we will pick our reference state to be the symmetric equilibrium solution, which we anticipate in case 1 when $\kappa = 1$. Thus, $\overline{S}_{21} = \overline{S}_{23} = S_{210} = S_{230}$, $\overline{S}_{24} = 1$, $\overline{q}_1 = \overline{q}_2$, and in fact the equations are now satisfied trivially by the solution $z = q = \phi_N + \phi_S = 1$, and $h = h_0$. One can put this solution in dimensional form by taking the previously specified ΔS and picking k and h_0 so as to tune the overturning circulation's strength and the thermocline depth to appropriate values. Appropriate choices would be those from the symmetric solution found by Marotzke and Klinger (2000). In their solution, $h \simeq 0.1$, $r \simeq 0.2$, and the total overturning is 26 Sv. If we take our basin volume to be

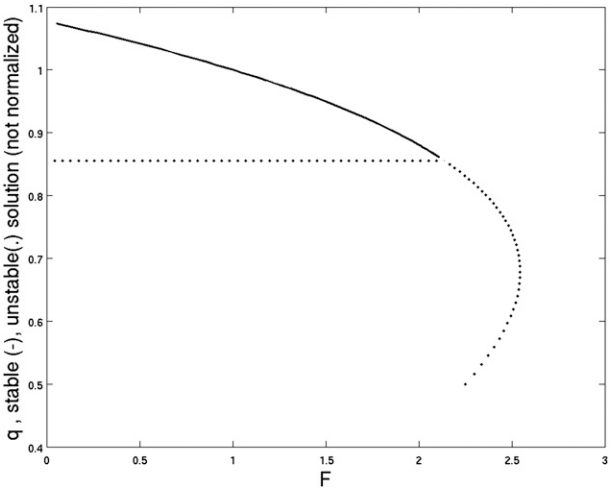

FIG. 2. Constant diffusivity equilibrium solution in case 1 for the total upwelling in low latitudes, q, vs the total poleward moisture flux, F, with symmetric forcing, $\kappa = 1$. The solid curve indicates stable solutions; the dotted curve unstable solutions.

the same as theirs, this yields a value of $k = 8 \times 10^{-8}$ s^{-1}. Finally we note that because we have chosen a symmetric state for our reference state, $l \equiv 1$.

For the case of symmetric forcing, $\kappa = 1$, and constant diffusivity, $n = 0$, Fig. 2 shows the solutions for the normalized total circulation strength, q, versus the total normalized salinity flux, F:

$$F \equiv \phi_N + \phi_S. \tag{48}$$

Figure 3 shows the corresponding solution for the constant energy case, $n = 1$. Because of our normalization, $q = 1$ when $F = 1$ in both cases. In both cases there is a single stable solution branch whose behavior is similar

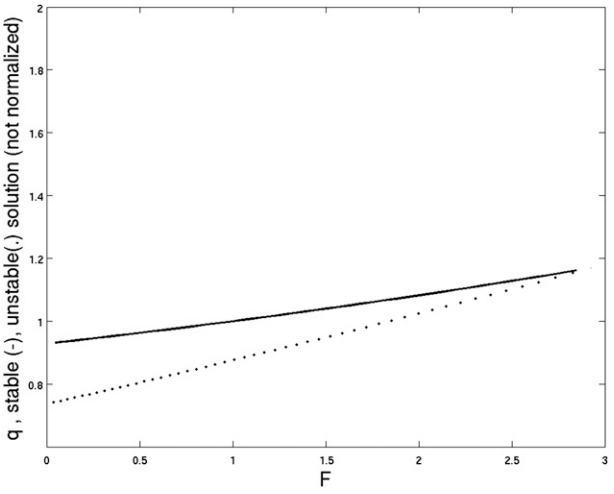

FIG. 3. Same as Fig. 2, but for the constant energy constraint.

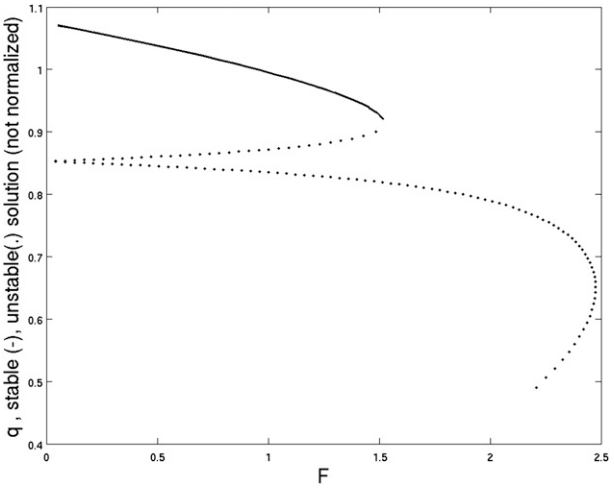

FIG. 4. Same as Fig. 2, but with $\kappa = 1.5$.

to that found by Nilsson et al. (2004) in their two-box model. In particular, q increases when F increases in the constant energy case, but decreases in the constant diffusivity case; stable solutions do not exist when F exceeds a critical value, or, equivalently, when the density contrast, S_{24}, exceeds a critical value. However, in addition we find a branch of unstable equilibrium solutions, also shown as the dotted curves in the figures. (The stability analysis will be discussed in the next section.) Finally, we note that the critical value of F is smaller in the case of constant diffusivity, as we would expect, and that $q_1 = q_2 = \frac{1}{2}q$ in both cases because of the symmetric forcing.

Figures 4 and 5 show the equilibrium solutions when the moisture flux forcing is asymmetric, $\kappa = 1.5$, for the constant diffusivity and energy cases, respectively.

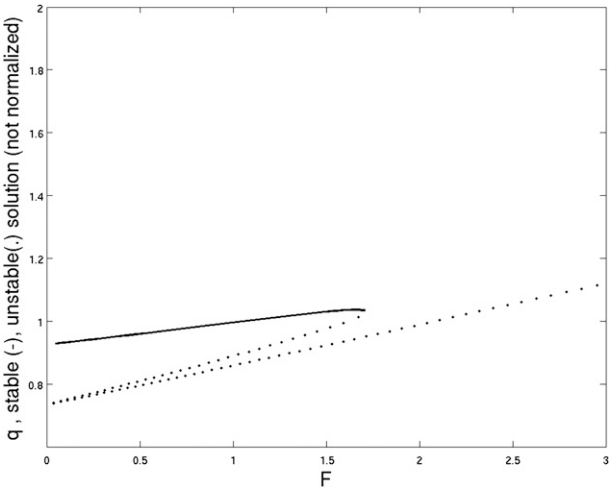

FIG. 5. Same as Fig. 3, but with $\kappa = 1.5$.

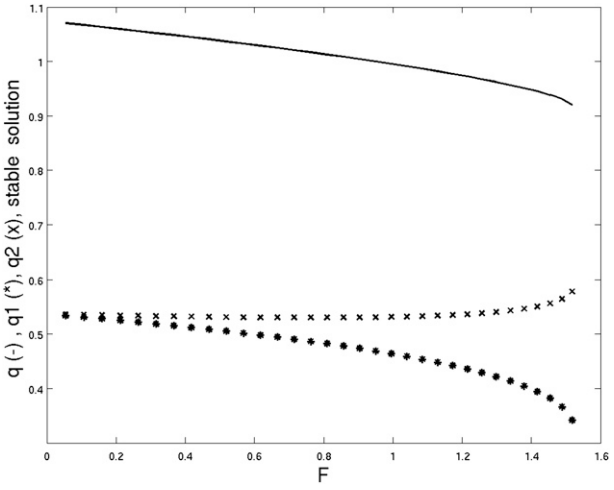

FIG. 6. Same as Fig. 4, but q_1 (asterisks) and q_2 (X's) as well as q (solid curve) are plotted vs F.

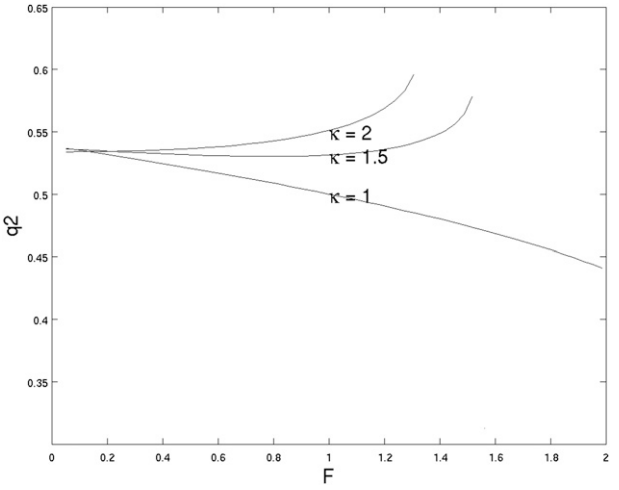

FIG. 8. The q_2 vs F for case 1 in the constant diffusivity case when $\kappa = 1$, 1.5, and 2.

Qualitatively the behavior is the same as when $\kappa = 1$, but now there is a second unstable branch, and the critical values of F are smaller. The hemispheric circulations for the stable solution are no longer identical, as shown in Figs. 6 and 7 for the constant diffusivity and energy cases, respectively. In this case, in contrast to the purely symmetric case, the trends in the two hemispheres as F increases have different signs, with the circulation increasing in the Southern Hemisphere and decreasing in the Northern Hemisphere in *both* cases. We note that the trends would be reversed if $\kappa < 1$.

In the constant diffusivity case, the trend in q_2—the circulation in the Southern Hemisphere—as F increases is reversed for large enough F compared to the case when $\kappa = 1$. When $\kappa = 1.5$, ϕ_S is relatively weaker and no longer controls the strength of the circulation in the Southern Hemisphere when F is large enough. Figure 8 shows how q_2 versus F depends on κ. For small F the trend is independent of κ, but when $\kappa > 1$ the trend eventually reverses as F approaches the critical value where instability sets in.

Similarly the trend in q_1 versus F in the constant energy case reverses for large enough F when $\kappa \geq 1.5$, as shown in Fig. 9. Thus in the constant energy case increasing moisture into high latitudes of the Northern Hemisphere can lead to a decreasing circulation in that hemisphere, just as in the constant diffusivity case, provided that the moisture flux into high northern latitudes is sufficiently stronger than that into high southern latitudes. This is in marked contrast to the behavior in

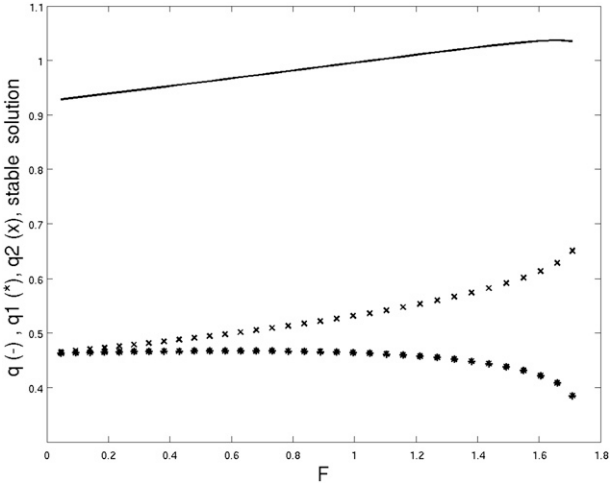

FIG. 7. Same as Fig. 6, but for the constant energy constraint.

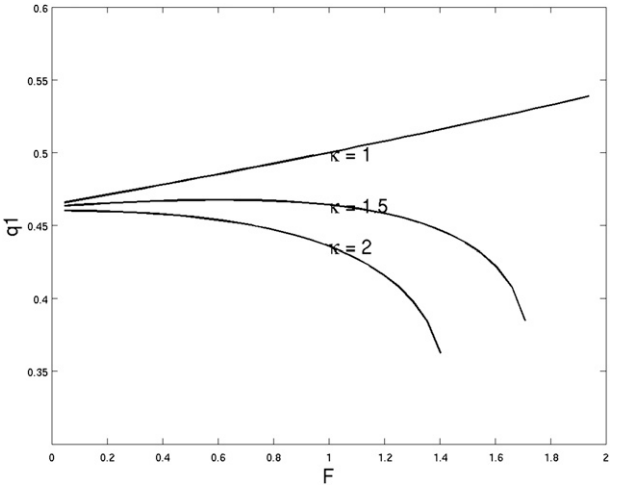

FIG. 9. The q_1 vs F for case 1 in the constant energy case when $\kappa = 1$, 1.5, and 2.

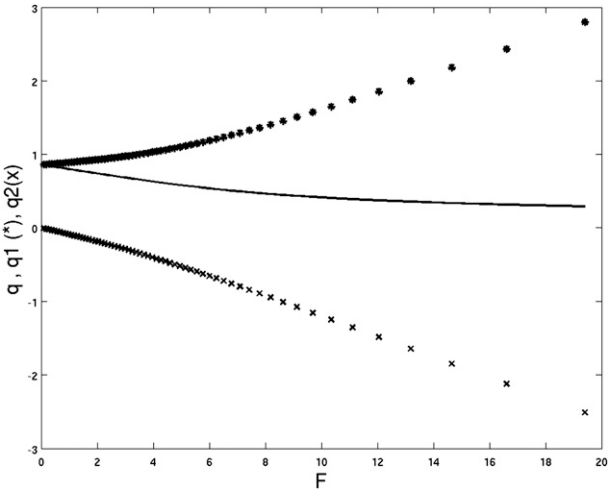

FIG. 10. Solution for q_1 (asterisks), q (solid curve), and q_2 (X's) vs F in case 2 for $\kappa = 1$ and constant diffusivity.

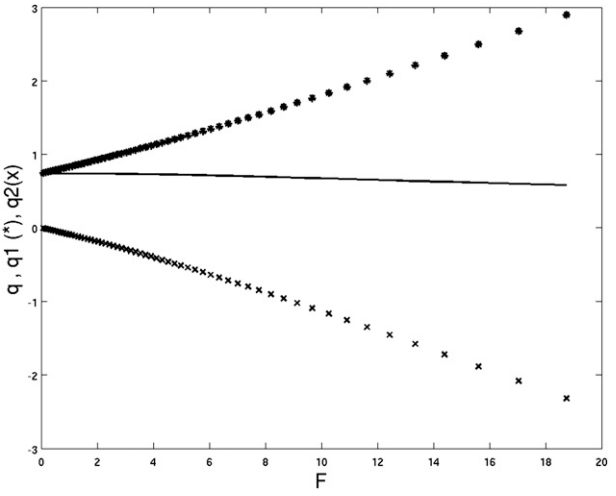

FIG. 11. Same as Fig. 10, but for constant energy.

the constant energy case in a hemispheric model or in an interhemispheric model with symmetric forcing.

The thermocline depth was normalized so that $h = h_0 = 0.1$ in case 1, when $F = \kappa = 1$. In fact, $h = h_0$ in case 1 when $F = 1$ for any κ. When F increases, h increases slowly for both the constant diffusivity and constant energy cases, and for either value of κ (results not shown).

b. Case 2

Now as we can see from Eqs. (16) and (33) the salinity in boxes 1 and 4 must be the same, $\overline{S}_{14} = 0$, and thus $\overline{S}_{43} = \overline{S}_{13}$ and $\overline{S}_{24} = \overline{S}_{21}$. Taking into account that $\overline{S}_{23} = \overline{S}_{21} + \overline{S}_{13}$, we find from Eqs. (35), (13), (26), (27), and (42) a quadratic equation for $\overline{S}_{13}$. The positive root,

$$\overline{S}_{13} = \frac{1}{2}\left(\frac{1 - r\overline{S}_{21}}{r}\right) + \sqrt{\left(\frac{1 - r\overline{S}_{21}}{2r}\right)^2 + \frac{1}{\kappa r}(1 - r\overline{S}_{21})\overline{S}_{21}}, \tag{49}$$

is consistent with the assumption $\overline{q}_1 > 0$, but the negative root is not. With this result all the salinity differences and h [from Eq. (37)] can be expressed in terms of $\overline{S}_{21}$ from Eqs. (25) and (27), and then combining all these results with the equilibrium conditions, Eqs. (31) and (14), we obtain a single equation for $\overline{S}_{21}$. The solutions must be checked to see that they satisfy the criteria $\overline{q}_1 > 0$, $\overline{q}_2 < 0$, and Eq. (47).

Figure 10 shows the solution for q, q_1, and q_2 versus F for $\kappa = 1$ and constant diffusivity. Figure 11 shows the solution for the same case but with the constant energy constraint. In both cases there is a single stable solution and the solutions are now stable for large values of F. These solutions are analogous to the solutions in the Rooth three-box model (Rooth 1982; see also Rahmstorf 1996), although there by construction $q_2 \equiv -q_1$. In fact for large F Rooth's assumed constraint is approximately satisfied by our solutions for both constant diffusivity and constant energy. Indeed in this limit the density contrasts forcing the circulation are proportional to the density contrast between the two high-latitude boxes, as assumed by Rooth (i.e., $\rho_{13} = 2\rho_{12} = -2\rho_{32}$). However, if $F \leq 0(1)$ we find in contrast that $|q_2| \ll q_1$ (i.e., there is only weak upwelling in the Southern Hemisphere). We also note that the total upwelling in the asymmetric solution when $F = 1$ is about 20% less than in the symmetric solution. This may be compared with Bryan's (1986) result "that approximately the same amount of deep water forms as in the symmetric case."

When the moisture flux into high latitudes increases in case 2, the interaction between the two hemispheres is quite different from that in case 1. In the case of constant diffusivity, in isolation the increased moisture flux would accelerate the upwelling in the Southern Hemisphere, but decrease the downwelling in the Northern Hemisphere. As shown in Fig. 10 in fact, the downwelling in the Northern Hemisphere increases. This is because the Southern Hemisphere circulation is transporting freshwater into low latitudes and this counteracts the effect of freshening in high northern latitudes on the density gradient. Since the circulation in the Southern Hemisphere increases more rapidly than that in the Northern Hemisphere as F increases, the tendency in the Northern Hemisphere is reversed, and the Southern Hemisphere dominates (i.e., q decreases as F increases). The Southern Hemisphere also has a dominant effect in

determining the strength of the northern downwelling in the Rooth (1982) model.

The solution for the constant energy constraint is very similar (Fig. 11). Now the tendency in the Northern Hemisphere is the same as one would expect in isolation, but in the Southern Hemisphere it is not, again because the freshwater transport in the Southern Hemisphere overcomes the tendency due to the surface flux. Again, as F increases the Southern Hemisphere dominates so that q now *decreases* (although very weakly), just the opposite of the behavior in case 1 and in the hemispheric models.

The solutions for case 2 when $\kappa = 1.5$ are virtually identical to those when $\kappa = 1$ (not shown). In the constant diffusivity case, q and q_1 are slightly less than when $\kappa = 1$, and slightly more in the constant energy case.

In case 2 for $F = 1$, $h = 0.11$ for any κ for both the constant diffusivity and constant energy, and h again increases slowly as F increases. In all cases, for sufficiently large F the thermocline collapses.

c. Case 3

The solution in this case closely follows that in case 2. Now $\overline{S}_{34} = 0$, and the analogous quadratic equation for $\overline{S}_{31}$ has a single root consistent with the assumption $\overline{q}_1 < 0$,

$$\overline{S}_{31} = \frac{1 - r\overline{S}_{23}}{2r} + \sqrt{\left(\frac{1 - r\overline{S}_{23}}{2r}\right)^2 + \frac{\kappa}{r}\overline{S}_{23}(1 - r\overline{S}_{23})}. \tag{50}$$

Again a single equation for $\overline{S}_{23}$ can be derived from the equilibrium conditions (31) and (14). The solution for $\kappa = 1$ is identical to that in case 2, except that the solutions for q_1 and q_2 are reversed. When $\kappa = 1.5$ the solutions are again very similar to those for $\kappa = 1$, but now in the constant diffusivity case q and q_1 are slightly less (algebraically) when $\kappa = 1.5$ than when $\kappa = 1$ in both the constant diffusivity and constant energy cases. The behavior of h is like that for case 2.

4. Stability analysis

a. Small perturbations

We first analyze the stability of the equilibrium solutions by considering infinitesimal perturbations. The loss of stability of the symmetric thermohaline circulation was explored by Nilsson et al. (2004), who found that it is always unstable to antisymmetric perturbations if $\beta(S_2 - S_4) > 0.5\alpha\Delta T$. We carried out a conventional analysis of the linearized perturbation equations and explored the eigenvalues for the asymmetric solutions as well as the symmetric solutions. Numerical solutions of the eigenvalue problem showed that the dotted solutions plotted in Figs. 2–5 were unstable equilibria, and that in general there were no stable solutions in case 1 when F is sufficiently large.

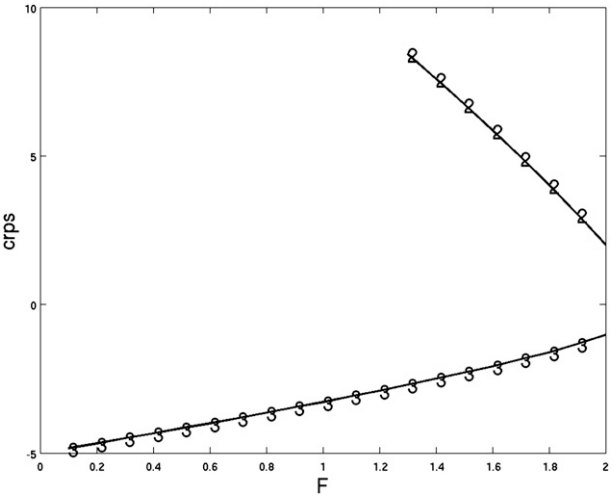

FIG. 12. Critical perturbations of S_1 (nondimensional units) that cause the equilibrium solution in case 1 to switch to another state, vs F, for the constant diffusivity case when $\kappa = 1$. The numbers on the curves indicate the kind of state it switches to, either case 2 or case 3.

b. Finite perturbations

We next investigate the stability of the equilibrium solutions to finite perturbations by introducing perturbations to the salinities in boxes 1 and 3. We integrate the nondimensional Eqs. (20)–(24) using a Runge–Kutta third-order scheme. We define the critical salinity perturbation to be the maximum perturbation (either positive or negative) for which the system will return to its original equilibrium state.

1) CASE 1

Figure 12 shows the critical perturbation of S_1 for case 1 when $\kappa = 1$ for constant diffusivity. The results for constant energy are very similar (not shown). We recall that the salinities and therefore the salinity perturbations have been scaled by a typical low-latitude vertical density difference, ΔS, and that a realistic choice would be $\Delta S = 0.5$ psu. For sufficiently large positive perturbations the solution with downwelling in high latitudes of both hemispheres (case 1) switches to a solution with upwelling in southern high latitudes (case 2). For sufficiently large negative perturbations it switches to one with upwelling in high northern latitudes (case 3). The constant energy case is somewhat more stable. When S_3

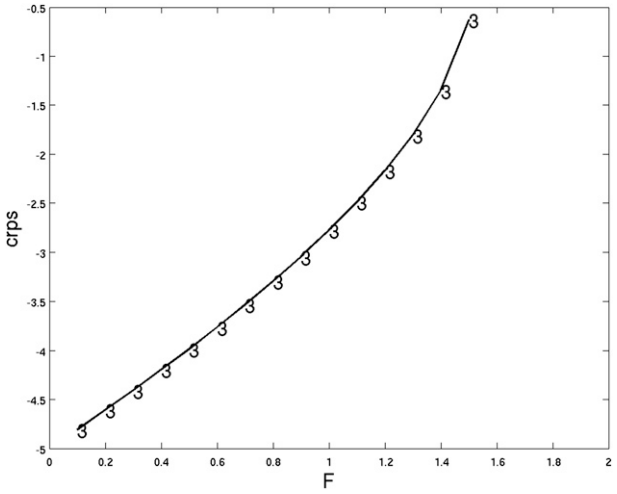

FIG. 13. Same as Fig. 12, but $\kappa = 1.5$.

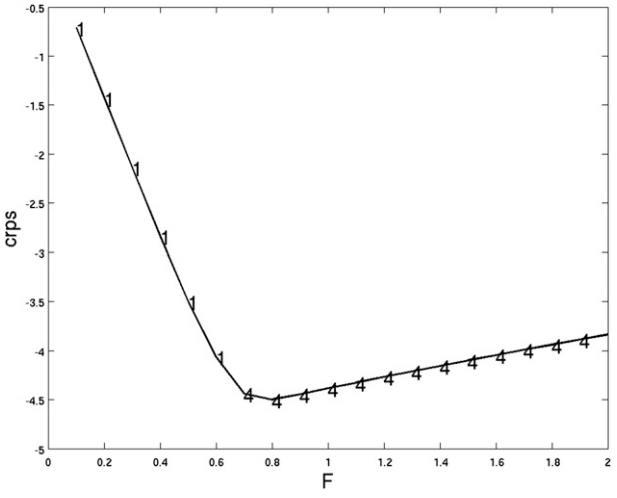

FIG. 14. Critical perturbation of S_1 vs F for case 2 for the constant diffusivity case when $\kappa = 1$. The number 4 indicates a transition to perturbations where $h \rightarrow 1$ and the model breaks down.

is perturbed instead of S_1 the critical values are identical to those found when S_1 was perturbed (results not shown) because the case 1 solution is perfectly symmetric when $\kappa = 1$. However, now large positive perturbations cause a switch to case 3, and negative perturbations to case 2.

Figure 13 shows the critical perturbations in S_1 for case 1 with $\kappa = 1.5$ for the constant diffusivity assumption. Again the results for the two assumptions are similar, with the constant energy case being slightly more stable (results not shown). Only negative perturbations can be unstable, unlike the behavior when $\kappa = 1$. However, when we perturb S_3 instead of S_1 (results not shown) the behavior is more like that when $\kappa = 1$ (Fig. 12), but the final states are reversed, because the stronger moisture flux into high southern latitudes favors a switch to upwelling there.

2) CASE 2

Figure 14 illustrates the critical S_1 perturbations in case 2 when $\kappa = 1$ for the constant diffusivity case. The results are very similar in the constant energy case, with the results being marginally more stable (not shown). In case 2, the equilibrium solutions are unstable only for negative S_1 perturbations. For smaller values of F, the system passes to states like those in case 1 when the critical perturbations are exceeded. However, for larger values of F the supercritical perturbations lead to a collapse of the thermocline ($h \rightarrow 1$) and the model breaks down. This behavior is indicated by the number fours in the figure.

Figure 15 plots the critical perturbations of S_3 versus F for the constant diffusivity case. In this case only positive perturbations lead to instability, and the system passes to a case 1 solution. The stability characteristics for the two constraints are again very similar, but in this case the constant energy case is slightly less stable (results not shown). In both cases, for large enough values of F, supercritical perturbations lead to a collapse of the thermocline (not shown).

When $\kappa = 1.5$, the stability of the two sets of equilibrium solutions to perturbations in S_1 are very similar to that when $\kappa = 1$, although the solutions are slightly less stable (results not shown). The stability to perturbations in S_3 is also very similar to the $\kappa = 1$ case when $\kappa = 1.5$. Again the stability is slightly less when $\kappa = 1.5$, and also now for larger values of F the system passes to a case 3 state rather than a case 1 state, both in the constant diffusivity case and the constant energy case.

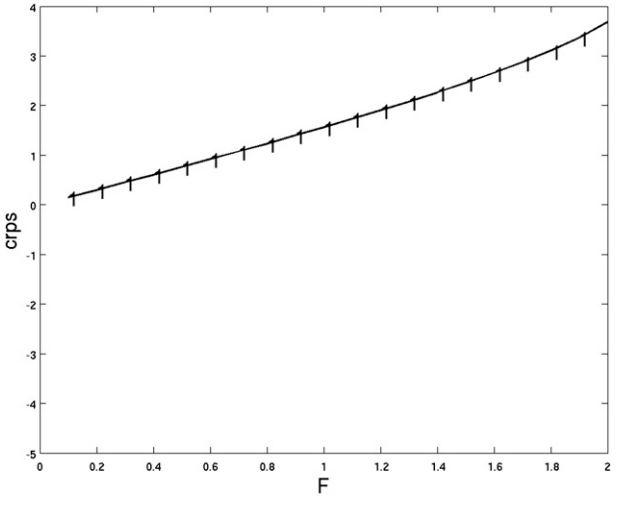

FIG. 15. Same as Fig. 14, but critical perturbations in S_3.

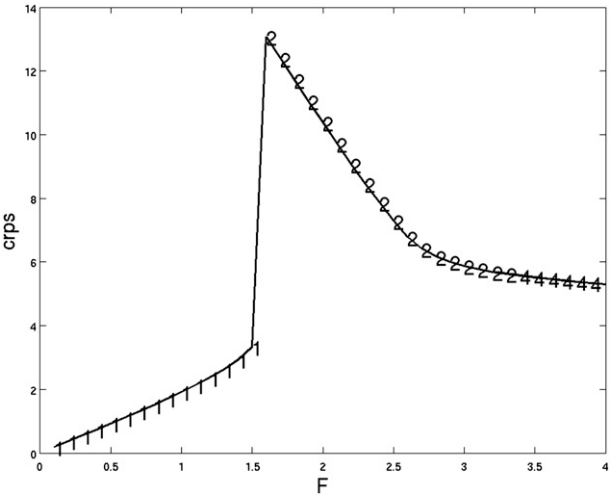

FIG. 16. Critical perturbation in S_1 for case 3 when $\kappa = 1.5$ for the constant diffusivity case.

Again, for sufficiently large F, the supercritical perturbations lead to a collapse of the thermocline.

3) CASE 3

When $\kappa = 1$, because of the symmetry of the forcing, the results for case 3 are identical to those for case 2, if the perturbations in S_1 are replaced by perturbations in S_3, and vice versa. Thus we do not show these results. When $\kappa = 1.5$, the results for perturbations in S_3 are very similar to those for $\kappa = 1$, although the $\kappa = 1.5$ case is a little more stable (results not shown). However, when $\kappa = 1.5$ the results for perturbations in S_1 are noticeably different, and are shown in Fig. 16 for the constant diffusivity case. The system is more stable than in case 2. (These perturbations in S_1 should be compared to those in S_3 for case 2 when $\kappa = 1.5$; shown in Fig. 15). The regime changes are similar for small F, with sufficiently large positive perturbations leading to a change from a case 3 solution to a case 1 solution, but for larger F the perturbations lead to a case 2 solution. In addition for larger F, the critical perturbations now decrease as F increases. This is caused by the asymmetry in the north/south moisture fluxes, which favors instability in case 3 for perturbations in S_1. For very large F the supercritical perturbations again lead to a collapse of the thermocline (results not shown). The results for the constant energy case are again very similar to those for constant diffusivity, but again this case is slightly more stable.

5. Hysteresis experiments

The above results imply that the model's equilibrium states are also unstable with changes in the surface moisture fluxes. Indeed, paleoclimatic evidence suggests that there may have been major changes in the Atlantic's MOC in the past in response to changes in the moisture flux into the North Atlantic (Broecker 2003). How the circulation in the current climate changes in response to changes in the moisture flux has been described in models that assume constant diffusivity by hysteresis experiments (Rahmstorf 1995; Rahmstorf et al. 2005). In these experiments the moisture flux into high latitudes is slowly increased until the circulation collapses, and then the flux is slowly decreased until the system recovers to its original state.

If such an experiment is performed in a hemispheric model with the assumption of constant energy, then the circulation increases indefinitely rather than collapsing (Nilsson and Walin 2001). However, our results in sections 3 and 4 suggest that the behavior when one assumes constant energy in our interhemispheric model will be like that when one assumes constant diffusivity. To verify this we carried out hysteresis experiments in which the initial state was one of the equilibrium states described in section 3. In these experiments we followed the standard procedure in which the moisture flux into the northern high-latitude box is enhanced by an amount $\Delta\phi$ (Rahmstorf et al. 2005). Thus Eq. (20) is replaced by

$$\frac{dS_1}{dt} = Q_1 - \phi_N - \Delta\phi, \tag{51}$$

and the other equations are unchanged.

If $\Delta\phi \neq 0$, then salinity is no longer conserved, and there is no true equilibrium. However, for a given, nonzero value of $\Delta\phi$, the *circulation* does reach an equilibrium. This can be shown by first defining the global mean salinity, S_T, as

$$S_T = \frac{1}{2+V}\left[S_1 + hVS_2 + S_3 + (1-h)VS_4\right], \tag{52}$$

and then adding Eqs. (20)–(23) together with appropriate weightings to derive the conservation equation for S_T. The result is

$$\frac{dS_T}{dt} = \frac{-\Delta\phi}{2+V} \equiv \sigma, \tag{53}$$

which has the simple solution

$$S_T = S_0 + \sigma t. \tag{54}$$

If we now define $S_i' = S_i - S_T$, $i = 1, 2, 3, 4$, then Eqs. (51) and (21)–(23) become

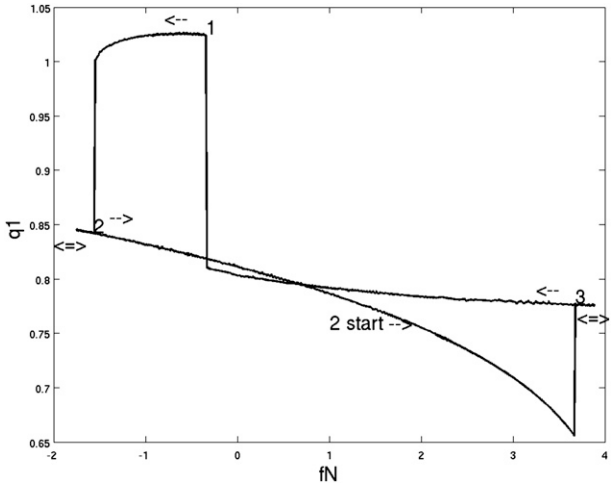

FIG. 17. The q vs fN when the initial state is the case 2 equilibrium state with $\kappa = 1.5$ and constant diffusivity. The numbers at the transitions indicate the kind of equilibrium state that the system transits to. The progression is $2 \rightarrow 3 \rightarrow 1 \rightarrow 2$.

$$\frac{dS_1'}{dt} = Q_1 - \phi_N - \Delta\phi - \sigma, \tag{55}$$

$$\frac{dS_2'}{dt} = \frac{1}{hV}(Q_2 + \phi_N + \phi_S) - \sigma, \tag{56}$$

$$\frac{dS_3'}{dt} = Q_3 - \phi_S - \sigma, \tag{57}$$

and

$$\frac{dS_4'}{dt} = \frac{1}{(1-h)V} Q_4 - \sigma. \tag{58}$$

These equations conserve the global salinity perturbation, and thus have steady solutions that are identical to those derived in section 3 when $\sigma = 0$, and closely analogous solutions when $\sigma \neq 0$.

Consequently, in the hysteresis experiments when $\Delta\phi$ is changed slowly enough, the circulation evolves through a series of quasi-equilibrium states, given by Eqs. (55)–(57) and (24). If at some point the circulation switched to a different regime, then subsequently $\Delta\phi$ was slowly decreased until the circulation returned to its original regime. Then $\Delta\phi$ was again slowly increased so as to complete the hysteresis loop.

Figure 17 shows how q changes in the constant diffusivity case when the initial state is case 2 with asymmetric forcing, $\kappa = 1.5$. Thus, initially $F = 1$, $\phi_S = 0.4$, $\phi_N = 0.6$, $q_1 = 0.87$, and $q_2 = -0.09$. We pick this solution as being the one most like the current climate in the Atlantic. Strength q is plotted versus the flux into the northern high-latitude box normalized by its initial value, that is, versus

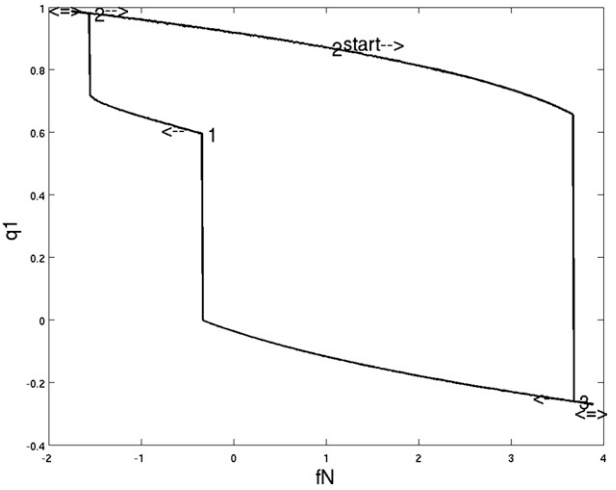

FIG. 18. Same as Fig. 17, but q_1 is plotted instead of q.

$$fN = \frac{\phi_N + \Delta\phi}{\phi_N}. \tag{59}$$

Figures 18 and 19 show how q_1 and q_2 change, respectively, in this case as fN first increases and then decreases. We see that as fN increases q_1 and q decrease, while q_2 increases (i.e., bottom water formation is being reduced in the Northern Hemisphere by the freshening); this causes the thermocline to deepen, and this in turn causes an increased circulation in the Southern Hemisphere. The first effect dominates so the total circulation is decreased. When fN reaches approximately 3.7, the circulation becomes unstable, and goes over to a new state corresponding to case 3 (i.e., now all the bottom water formation is in the Southern Hemisphere). If fN now starts to decrease, the system remains in the new

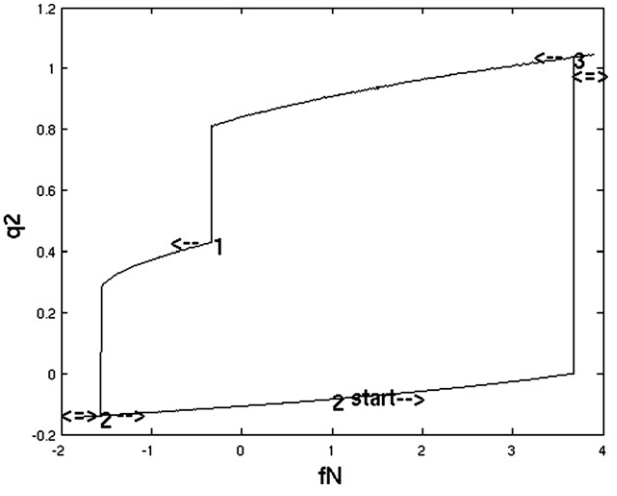

FIG. 19. Same as Fig. 18, but q_2 is plotted instead of q_1.

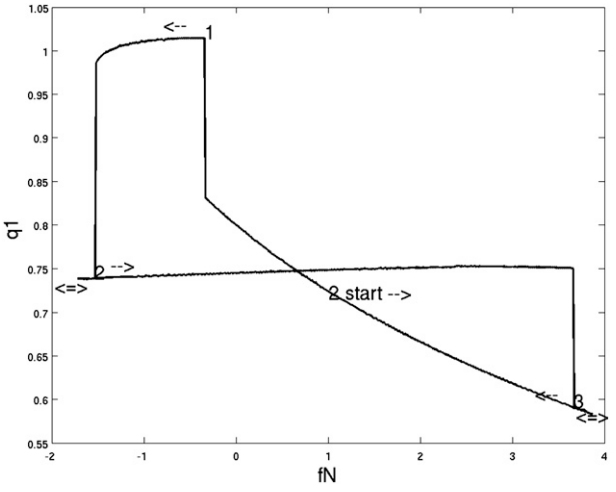

FIG. 20. Same as Fig. 17, but for the case of constant energy.

regime until fN changes sign and reaches about -0.3. Now the increased salinity in the Northern Hemisphere becomes large enough that bottom water formation sets in once again, and the system changes to a case 1 state, with bottom water formation in both hemispheres. If fN continues to decrease, eventually the system returns to the case 2 regime.

Note that the solution on the case 3 branch when $fN = 1$ ($\Delta\phi = 0$) corresponds to the (true) equilibrium solution for case 3 when $\kappa = 1.5$ and $F = 1$. If we started the hysteresis experiment from this point, then the system would trace out the same series of loops, but in a counterclockwise direction. The behavior for $fN > 0$ is very similar to that of the Rooth (1982) model and the more sophisticated models examined by Rahmstorf et al. (2005).

Figures 20, 21, and 22 show the hysteresis loops for q, q_1, and q_2, respectively, for the case of constant energy when starting from the case 2 equilibrium state with $\kappa = 1.5$ and $F = 1$. In this case the initial state has $q_1 = 0.82$, $q_2 = -0.07$. Comparing with Figs. 17–19, we see that the behavior is very similar. In particular q_1 still decreases initially, in accord with Marzeion et al.'s (2007) result with their global OGCM. One quantitative difference is that the initial decrease in q_1 is weaker in the constant energy case (cf. Figs. 18 and 21), and consequently q increases weakly in this case whereas it decreases weakly in the constant diffusivity case (cf. Figs. 17 and 20). Nevertheless, the circulation eventually collapses in both cases from a circulation with all bottom water formation in the Northern Hemisphere to one with bottom water formation only in the Southern Hemisphere, and in both cases this occurs for $fN = 3.7$.

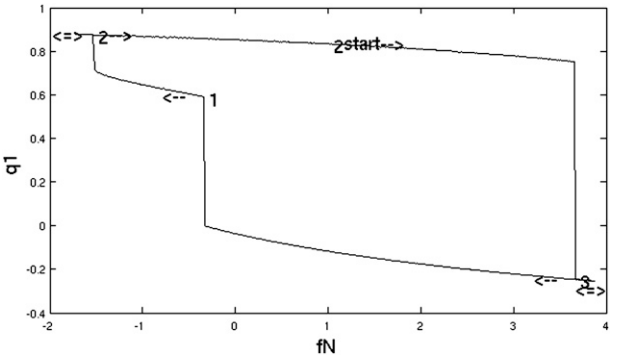

FIG. 21. Same as Fig. 18, but for the case of constant energy.

6. Summary and discussion

We have constructed an interhemispheric four-box model with one high-latitude box in each hemisphere and two low-latitude boxes—a surface box and a deep box—separated by a thermocline in which there is a balance between vertical advection and vertical diffusion. We have assumed fixed thermal forcing and investigated how the model's solutions depend on the hydrological forcing. Our analysis was carried out using two contrasting assumptions about how the vertical diffusivity changes when the hydrological forcing changes. In one case we make the conventional assumption that the diffusivity is constant, and in the other case, following Huang (1999) and Nilsson and Walin (2001), we assume that the energy input to the vertical mixing is constant.

The qualitative nature of the solution is mostly the same for both assumptions. As in Bryan's (1986) OGCM with a single interhemispheric basin there are three stable equilibrium solutions. Two are asymmetric and

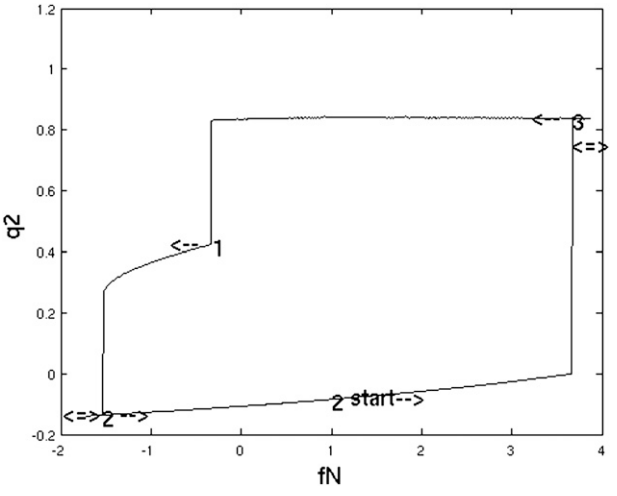

FIG. 22. Same as Fig. 19, but for the case of constant energy.

are analogous to the two solutions found by Rooth (1982) with downwelling in high latitudes of one or the other of the two hemispheres. In these solutions the downwelling is maintained by advection of salinity from low to high latitudes. These solutions are generally stable to small perturbations and exist for any strength of the global hydrological cycle, up to the point where the thermocline reaches the bottom of the ocean. There is also a stable, thermally dominated, quasi-symmetric solution analogous to the one described by Nilsson et al. (2004), with downwelling in high latitudes of both hemispheres. (This solution is perfectly symmetric when the forcing is symmetric.) There is no analog of this state in the Rooth (1982) model. This state becomes linearly unstable when the global hydrological forcing becomes strong. In addition, transitions between the three stable equilibrium states can be caused by appropriate finite amplitude salinity perturbations, although the required perturbations are relatively large unless the hydrological forcing is weak.

There are significant differences in the quasi-symmetric solution for the two different closure assumptions. As the hydrological forcing increases the total upwelling decreases for constant diffusivity and increases for constant energy, as in the hemispheric model of Nilsson et al. (2004). However, if the hydrological forcing is strongly asymmetric, the bottom water formation in the hemisphere with the weakest hydrological forcing will have changes opposite in sign to those in the other hemisphere and in the total upwelling. Also, in spite of the different trends in the total upwelling for the different assumptions, these solutions become unstable at about the same strength of the hydrological forcing and pass to asymmetric states. In the case of constant energy this is in marked contrast to the behavior in hemispheric box models and OGCMs where there is no such instability (Nilsson and Walin 2001; Nilsson et al. 2004).

For the asymmetric solutions there are only minor quantitative differences between the results with the two different assumptions. In both cases as the global hydrological forcing increases the bottom water formation in the hemisphere with sinking increases as in the Rooth model, but in contrast with the Rooth model no linear instability ever sets in. This behavior is similar to that in the hemispheric model case when constant energy is assumed, and just the opposite of the behavior when constant diffusivity is assumed. We note, however, that for both assumptions about the mixing when the bottom water formation increases in the sinking hemisphere the total upwelling in low latitudes nevertheless decreases, because the upwelling in the opposite hemisphere increases more rapidly. Thus for the asymmetric solutions the response to the hydrological forcing does not depend qualitatively on the assumption about the mixing, in contrast to the quasi-symmetric solution.

However, the asymmetric solutions can be destabilized by sufficiently large salinity perturbations. This behavior is similar to that in a hemispheric model with a constant diffusivity assumption, but contrary to the behavior in the hemispheric model with constant energy. This difference between the interhemispheric and hemispheric models is reflected in the hysteresis loops we calculated. For either assumption an asymmetric solution with sinking in one hemisphere can be switched to an asymmetric solution with sinking in the other hemisphere, or to a quasi-symmetric solution, depending on the perturbation in the hydrological forcing. By contrast, in the hemispheric model with the constant energy assumption, there are no such transitions and no hysteresis loop.

Perhaps our most interesting result is that the stability properties of the solutions in the interhemispheric model are qualitatively similar for the two different assumptions—constant diffusivity and constant energy. This is in marked contrast to the hemispheric case where there is stability for the constant energy assumption, but not for the constant diffusivity assumption.

Of course our model is very simple. Aside from the assumption of fixed temperatures, the boxes are assumed to be well mixed, there is no wind stress forcing, and there is a single basin. However, with respect to the first three of these simplifications, there are numerous studies that show that they do not affect the number of equilibrium solutions or the qualitative effect of changes in the hydrological forcing. These studies include ocean box models with interactive temperatures, coupled to atmospheric energy balance models (Nakamura et al. 1994; Marotzke 1996; Krasovskiy and Stone 1998; Scott et al. 1999), and OGCMs that in addition to having interactive temperatures are also forced by wind stresses and have interactive stratifications (Bryan 1986; Schiller et al. 1997; Wang et al. 1999a,b; Marzeion et al. 2007). Indeed, our results offer an explanation for the decrease of the Atlantic MOC in the global geometry experiment of Marzeion et al. with a constant energy constraint (i.e., it is because of the interhemispheric nature of the Atlantic MOC).

However, if the basin is not isolated, then significant differences do arise. For example, Marotzke and Willebrand (1991) used an OGCM to find the equilibrium states for an ocean consisting of two interhemispheric basins joined by a circumpolar current in one hemisphere. They used a fixed diffusivity and did find two asymmetric states similar to the two in our model; but in addition, they found two ''conveyor belt'' states that of course cannot exist in a single basin like ours. However,

like the behavior in our model, the strength of the meridional overturning in their model increases as the global hydrological cycle increases; a sufficiently large increase in moisture input to a single high-latitude sinking region causes the sinking to collapse and the circulation to change to a different state (Wang et al. 1999a).

The only study so far to look at the behavior of a multibasin model with the energy constraint is that of Marzeion et al. (2007). They used a realistic global geometry and also found that adding freshwater to downwelling in high latitudes of the North Atlantic caused a decrease of the circulation for either constraint. However, they did not look for multiple equilibria, and as yet, there has been no analysis of the behavior of all the possible states in a multibasin model when the energy constraint is used.

Acknowledgments. We are grateful for the constructive and insightful comments provided by Jeffery R. Scott and three anonymous reviewers, which led to significant improvements of the original manuscript.

REFERENCES

Broecker, W. S., 2003: Does the trigger for abrupt climate change reside in the ocean or in the atmosphere? *Science,* **300,** 1519–1522.

——, T.-P. Pend, J. Houzel, and G. Russell, 1990: The magnitude of global freshwater transports of importance to ocean circulation. *Climate Dyn.,* **4,** 73–79.

Bryan, F., 1986: High-latitude salinity effects and interhemispheric thermohaline circulations. *Nature,* **323,** 301–323.

Bugnion, V., C. Hill, and P. H. Stone, 2006: An adjoint analysis of the meridional overturning circulation in a hybrid coupled model. *J. Climate,* **19,** 3751–3767.

Ganachaud, A., and C. Wunsch, 2003: Large-scale ocean heat and freshwater transports during the World Ocean Circulation Experiment. *J. Climate,* **16,** 696–705.

Huang, R. X., 1999: Mixing and energetics of the oceanic thermohaline circulation. *J. Phys. Oceanogr.,* **29,** 727–746.

Krasovskiy, Y., and P. H. Stone, 1998: Destabilization of the thermohaline circulation by atmospheric transports: An analytic solution. *J. Climate,* **11,** 1803–1811.

Marotzke, J., 1996: *Analysis of Thermohaline Feedbacks*. NATO ASI Series, Vol. 144, Springer-Verlag, 378 pp.

——, and J. Willebrand, 1991: Multiple equilibria of the global thermohaline circulation. *J. Phys. Oceanogr.,* **21,** 1372–1385.

——, and B. A. Klinger, 2000: The dynamics of equatorially asymmetric thermohaline circulations. *J. Phys. Oceanogr.,* **30,** 955–970.

Marzeion, B., A. Levermann, and J. Mignot, 2007: The role of stratification-dependent mixing for the stability of the Atlantic overturning in a global climate model. *J. Phys. Oceanogr.,* **37,** 2672–2681.

Mohammad, R., and J. Nilsson, 2004: The role of diapycnal mixing for the equilibrium response of thermohaline circulation. *Ocean Dyn.,* **54,** 54–65.

Munk, W. H., and C. Wunsch, 1998: Abyssal recipes II: Energetics of tidal and wind mixing. *Deep-Sea Res. I,* **45,** 1977–2010.

Nakamura, M., P. H. Stone, and J. Marotzke, 1994: Destabilization of the thermohaline circulation by atmospheric eddy transports. *J. Climate,* **7,** 1870–1882.

Nilsson, J., and G. Walin, 2001: Freshwater forcing as a booster of thermohaline circulation. *Tellus,* **53A,** 628–640.

——, G. Broström, and G. Walin, 2003: The thermohaline circulation and vertical mixing: Does weaker density stratification give stronger overturning? *J. Phys. Oceanogr.,* **33,** 2781–2795.

——, ——, and ——, 2004: On the spontaneous transition to asymmetric thermohaline circulation. *Tellus,* **56A,** 68–78.

Rahmstorf, S., 1995: Bifurcation of the Atlantic thermohaline circulation in response to changes in the hydrological cycle. *Nature,* **378,** 145–149.

——, 1996: On the freshwater forcing and transport of the Atlantic thermohaline circulation. *Climate Dyn.,* **12,** 799–811.

——, and Coauthors, 2005: Thermohaline circulation hysteresis: A model intercomparison. *Geophys. Res. Lett.,* **32,** L23605, doi:10.1029/2005GL023655.

Rooth, C., 1982: Hydrology and ocean circulation. *Prog. Oceanogr.,* **11,** 131–149.

Schiller, A., U. Mikolajewicz, and R. Voss, 1997: The stability of the North Atlantic thermohaline circulation in a coupled ocean-atmosphere general circulation model. *Climate Dyn.,* **13,** 325–347.

Scott, J., and J. Marotzke, 2002: The location of diapycnal mixing and the meridional overturning circulation. *J. Phys. Oceanogr.,* **32,** 3578–3595.

——, ——, and P. H. Stone, 1999: Interhemispheric thermohaline circulation in a coupled box model. *J. Phys. Oceanogr.,* **29,** 351–365.

Seager, R., D. S. Battisti, J. Yin, N. Gordon, N. Naik, A. C. Clement, and M. A. Cane, 2002: Is the Gulf Stream responsible for Europe's mild winters? *Quart. J. Roy. Meteor. Soc.,* **128,** 2563–2586.

Stommel, H. M., 1961: Thermohaline convection with two stable regimes of flow. *Tellus,* **13,** 224–230.

Stouffer, R. J., and Coauthors, 2006: Investigating the causes of the response of the thermohaline circulation to past and future climate changes. *J. Climate,* **19,** 1365–1387.

Wang, X., P. H. Stone, and J. Marotzke, 1999a: Global thermohaline circulation. Part I: Sensitivity to atmospheric moisture transport. *J. Climate,* **12,** 71–82.

——, ——, and ——, 1999b: Global thermohaline circulation. Part II: Sensitivity with interactive atmospheric transports. *J. Climate,* **12,** 83–91.